Available online at www.sciencedirect.com
SCIENCE DIRECT
Polymer 46 (2005) 9133–9143
polymer
www.elsevier.com/locate/polymer

Highly ordered microstructures of poly(styrene-*b*-isoprene) block copolymers induced by solution meniscus

Jiyoung Hwang[a], June Huh[b], Bumsuk Jung[c], Jae-Min Hong[d], Min Park[e], Cheolmin Park[a,*]

[a]*Department of Materials Science and Engineering, Yonsei University, Seoul 120-749, South Korea*
[b]*School of Materials Science and Engineering, Seoul National University, Seoul, South Korea*
[c]*Department of Environmental Engineering and Biotechnology, Myongji University, san 38-2 Namdong, Yongin, Kyunggido 449-728, South Korea*
[d]*Optoelectronic Materials Center, Korea Institute of Science and Technology, P.O. Box 131, Cheongryang, Seoul 130-650, South Korea*
[e]*Polymer Hybrid Research Center, Korea Institute of Science and Technology, P.O. Box 131, Cheongryang, Seoul 130-650, South Korea*

Received 18 November 2004; received in revised form 15 June 2005; accepted 25 June 2005
Available online 10 August 2005

Abstract

Microstructures of hundreds of micron thick poly(styrene-*block*-isoprene) copolymer films solution-cast in a cylindrical tube with the solvent evaporation controlled were investigated by transmission electron microscope (TEM), small angle X-ray scattering (SAXS) and optical microscope (OM). In a block copolymer with cylindrical polyisoprene microdomains, the orientation of the cylinders was varied along radial direction of the cylindrical tube. Highly aligned hexagonal arrays of in-plane polyisoprene cylinders were formed with their cylindrical axis parallel to the circumference of the tube in the regimes close to the wall edge. In contrast randomly ordered microdomains were observed at the center of the tube. We have also found that the orientation depends on the solvent evaporation rate and an intermediate rate ($\sim$2.3 nL/s) provides the best orientation. In the case of a block copolymer with a bicontinuous double gyroid structure, we obtained a globally ordered microstructure where [111] crystallographic direction was parallel to the circumference of the tube. For both block copolymers, the area of highly ordered arrays of nanoscopic domains is over 1 mm^2. Development of the orientation was explained by coupling two orthogonal fields: (1) The flow of a solution induced by strong capillary force at a meniscus between the cylindrical tube wall and the block copolymer solution and (2) the solvent evaporation.

Keywords: Poly(styrene-*b*-isoprene) block copolymer; Microstructure orientation; Solution meniscus

1. Introduction

Self assembly of block copolymers produces microstructures on the nanoscopic length scale. The interplay of frequently occurring incompatibility between the constituent blocks and the fact that they are covalently connected on a molecular level give rise to a variety of ordered microdomain structures in the thermal equilibrium [1,2].

Well ordered block copolymer nanostructures provide a simple route to nanoscopic templates that find uses in nanotechnological applications such as ultrahigh density storage media, nanoporous ceramic membrane, photonic crystals and quantum dot arrays [2,3]. However, perfect periodic domain ordering can only be achieved over micrometer scale area and defects exist at the edges of grain boundaries. It is, therefore, essential that both the orientation and lateral ordering of the nanoscopic domains be controlled to fully realize the potential of these materials. Several techniques are currently used for inducing alignment of the microdomains in block copolymers [2,3]. They rely on the ability to couple an externally applied field to some molecular and/or supermolecular feature in the polymer and thus achieve directional properties, such as transport, optical, and mechanical properties.

Many schemes have been developed for control of the arrangement of microdomains in block copolymer films. These include the use of applied electrical [4–6], mechanical fields [7–9], solvent evaporation [10–14], graphoepitaxy [15–18] and temperature gradient [19,20]. Although these directional forces have been effective in controlling

* Corresponding author. Tel.: +82 2123 2833; fax: +82 312 5375.
E-mail address: cmpark@yonsei.ac.kr (C. Park).

0032-3861/$ - see front matter © 2005 Elsevier Ltd. All rights reserved.
doi:10.1016/j.polymer.2005.06.070

two dimensional domain alignments, attaining highly ordered arrays with the long range lateral order requires coupling of more than one field in orthogonal directions. For instance, controlled microdomain structures of block copolymers in thin films were obtained by using a crystallizable solvent where biaxial forces: Directional crystallization and solvent evaporation were played [21,22]. We have also employed confined directional crystallization of a crystallizable solvent in combination with topographically patterned substrates to create a double orientation with controlled lattice orientation of the minority microdomains [23].

Solvent evaporation is also a strong, directional field [10–14]. The solvent evaporation rate is one of the key factors that determine kinetically arrested nanostructures. With the proper preparation conditions, the solvent concentration gradient became maximized along the direction perpendicular to the film surface [10,12], resulting in a cylindrical microdomain orientation perpendicular to the film surface. In these methods, however, the lateral registry of the cylinders is poor, since the gradient of solvent concentration is uniaxial and the *P6mm* structure of the cylindrical microdomain is degenerate under this force.

Krausch et al. showed that solvent annealing could remarkably improve the ordering of block copolymer morphologies in thin films [11]. By controlling the rate of solvent evaporation with solvent annealing, ordering induced at the surface propagated through the entire film. Recently, Kimura et al. have demonstrated that long range order in arrays of cylindrical microdomains oriented parallel to the surface can be achieved by pinning a solution droplet on a substrate [14,24]. They have utilized two orthogonal fields: A strong flow of the solution within the droplet directed toward the pinned edge and an ordering front that initiates at the surface and propagates into the droplet. Furthermore, Kim et al. realized long range lateral ordering of vertically oriented cylindrical microdomains by combining directional solvent evaporation with micropatterned substrates [13].

This paper describes a new and simple method to produce globally ordered nanostructures of poly(styrene-*block*-isoprene) block copolymers. The method is based on quiescently casting block copolymer solutions confined in a cylindrical tube with a diameter of 8 mm under controlled solvent evaporation. There exist two orthogonal external fields during the solution cast. One is the flow of a solution toward the tube wall induced by strong capillary force at a meniscus between the cylinder wall and the block copolymer solution. The other is solvent evaporation that makes an ordering front start at the surface and propagate into the solution. These coupled biaxial forces produce highly aligned ordered arrays of in-plane cylindrical microdomains with their cylindrical axis parallel to the perimeter of the casting tube. We also demonstrate that our method is very effective to produce an oriented gyroid nanostructure with a nearly single grain of 1 m^2 in area.

2. Experimental section

2.1. Materials

We use two polystyrene-*block*-polyisoprene diblock copolymers: PS/PI(45/12) and PS/PI(44/19). PS/PI (45/12) has a total molecular weight of 57,000 g/mol, a polydispersity of 1.06, with PS and PI blocks of 45,000 and 12,000 g/mol, respectively. This sample presents a bulk cylindrical microstructure evidenced by small-angle X-ray scattering (SAXS: $d_{10\ \mathrm{cyl}} \sim 35$ nm), consistent with the 75% volume fraction of the PS block. PS/PI (44/19) has a total molecular weight of 63,000 g/mol with PS and PI blocks of 44,000 and 12,000 g/mol, respectively (PDI = 1.07). Since the volume fraction of the PI block is 35%, the bulk sample displays a bicontinuous double gyroid microstructure (evidenced by SAXS: $d_{211\ \mathrm{gyroid}} \sim 42$ nm). Both block copolymers were supplied by Dr Fetters at Cornell University.

2.2. Film preparation

The thick films of either PS/PI (45/12) or PS/PI (44/19) block copolymer were prepared by quiescently casting a 5 wt% solution (solvent: toluene) in a cylindrical tube that has 8 mm in diameter, 20 mm in height. A meniscus of the block copolymer solution was formed with a non-zero contact angle on the tube wall. The contact angle was determined by the balance of the forces at the line of contact between the solution and the wall. The solvent evaporation was controlled by covering a cap with holes (diameter is approximately 2 mm) (Fig. 1(a)). The film formation was performed at room temperature. The films were dried in a vacuum oven at 40 °C for 24 h in order to remove all traces of the solvent. No further annealing was made. We used a cylindrical coordinate in which the tube axis corresponds to *Z*, tube radius to *R*. The evaporation rate was determined by measuring the initial volume of a block copolymer solution and the time required for the volume change. Three different solvent evaporation rates were used. A fast evaporation rate was approximately 200 nL/s. An intermediate ($\sim$2.3 nL/s) and a slow ($\sim$0.1 nL/s) evaporation rate were used to prepare the films. It took 5 and 30 days to complete film formation with the intermediate and the slow evaporation, respectively. The thickness of the cast films was approximately 0.5 mm.

2.3. Small angle X-ray scattering (SAXS)

The small angle X-ray scattering (SAXS) measurements with synchrotron radiation were conducted at the 4C2 beam line at the Pohang Light Source (Korea) where W/B4C double multilayer monochromator delivered monochromatized X-rays with a wavelength of 0.1608 nm and an energy resolution of 0.01 (E/E) onto the sample. Scattering angles, 2θ down to 1.5 mrad corresponding to a Bragg spacing

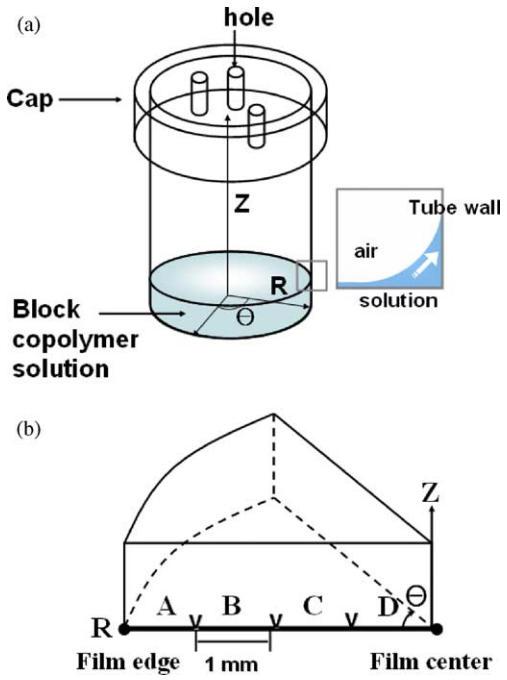

Fig. 1. (a) Schematic diagram of cylindrical casting tube (diameter: 8 mm) and cylindrical coordinate used. The holes (diameter: 2 mm) on the cap are used to control the solvent evaporation. A meniscus formed at the contact line between a tube wall and a block copolymer solution is also shown. (b) The sample positions at which X-ray scattering and optical microscope were performed.

($d=2\pi/q$ where $q=4\pi \sin\theta/\lambda$) of about 100 nm were achieved. A flat Au mirror was used to eliminate the higher harmonics from the multilayer monochromator. A 2D CCD camera (Princeton Instruments Inc., SCX-TE/CCD-1242) was used to collect the scattered X-rays.

The degree of alignment of the cylinders was quantified using the second-order orientation factor, F_2 [25]. The intensity was integrated as a function of the azimuthal angle, ϕ in a ring about the principal peak wavevector q^*, with a width given by the full width at half maximum of the primary peak, resulting in the scattered intensity as a function of angle, $I(q^*,\phi)$ ($\phi=0°$ at the peak in intensity). The normalized orientation distribution function of the cylinder axes is

$$P(\phi) = \frac{I(q^*,\phi)q^{*^2}}{\int_0^{\pi} I(q^*,\phi)q^{*^2}\sin\phi \mathrm{d}\phi} \quad (1)$$

The second-order orientation factor is given as

$$F_2 = 1 - 3\langle\cos^2\phi\rangle \quad (2)$$

where $\langle\cos^2\phi\rangle$ is

$$\langle\cos^2\phi\rangle = \int_0^{\pi} \cos^2\phi P(\phi)\sin\phi \mathrm{d}\phi \quad (3)$$

If the cylinders were perfectly aligned, $P(\phi)$ would be a delta function at 0° and $F_2=1$. If the alignment is isotropic, $P(\phi)$ is independent of ϕ and $F_2=0$.

2.4. Polarized optical microscopy

Optical microscope (Olympus BX51M) was used for examining the cast films under crossed polarizers. The images were recorded with a CCD (Pixeline, PL-A662).

2.5. Transmission electron microscopy

Cryogenic ultrathin sectioning was performed with a Reica ultracut-S cryotome at −100 °C. Some samples were stained selectively with an aqueous 4 wt% OsO_4, a preferential stain for the PI block, for several hours. The bright field TEM was then performed for the samples with JEOL JEM-2010, JEOL JEM-3011 operated at 120 kV. Fast Fourier transformation (FFT) were made from the TEM images, using a software, Scion Image.

3. Result and discussion

Fig. 2 shows the SAXS patterns of PS/PI(45/12) sample cast with the intermediate evaporation rate (~2.3 nL/s) with the incident beam parallel to the Z direction. Four different regions that correspond to ones indicated in Fig. 1(b) were examined. Only the first order reflection corresponding to (10) one for each SAXS pattern was shown for comparison. The value of the scattering vector of the first peak ($q_1=0.18\ \mathrm{nm}^{-1}$) indicates that the hexagonal lattice has a periodicity of 35 nm. It is apparent that the best orientation of the cylinder microdomains occurred at the region A. Table 1 lists the F_2 value for each region shown in Fig. 1. The F_2 value for each region is obtained by averaging the values from several different positions in each region. The F_2 value obtained at the region A is 0.89. The orientation decreases toward the center of the tube and the microdomains become random in orientation at the center finally. The F_2 value is almost zero at region D. We found that the in-plane cylindrical PI domains were oriented parallel to the perimeter of the cylindrical tube.

The orientation developed in the solution cast PS/PI (45/12) films was also confirmed by OM under crossed polarizers. Fig. 3 shows the thickness normalized OM micrographs of PS/PI (45/12) film. The global orientation of the cylindrical microdomains resulted in form birefringence. The retardation defined by the product of birefringence and film thickness allowed the incident visible light to pass through the cross polarizers. The highest brightness

Table 1
F_2 for each region indicated in Fig. 1(b)

Sample position	F_2
A	0.89
B	0.65
C	0.4
D	0.05

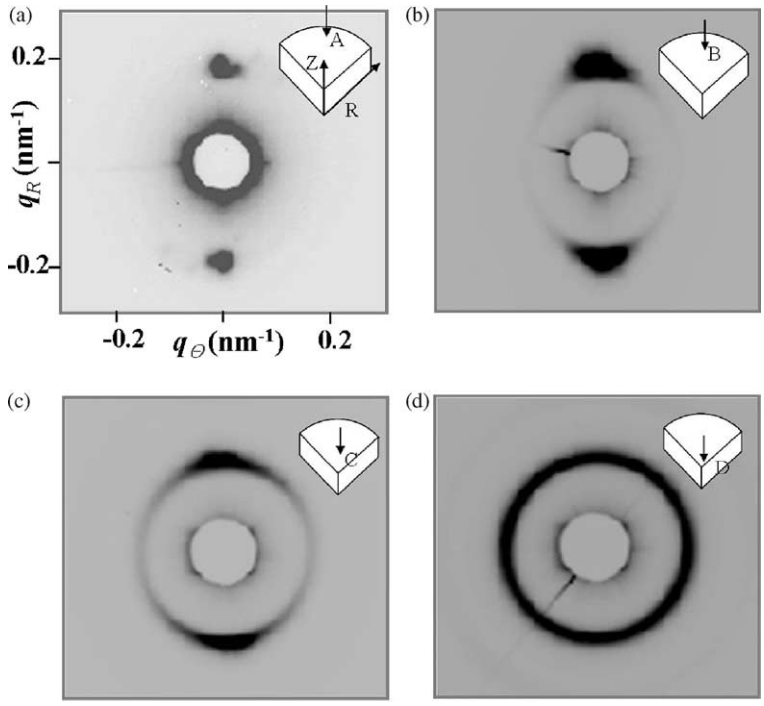

Fig. 2. 2D SAXS patterns of the solution cast PS/PI (45/12) sample with the incident beam parallel to the *Z* direction. The scattering patterns detected from 4 regions along the radial direction as depicted in Fig. 1(b) are shown. The maximum orientation is obtained at the wall of the tube (a). The orientation is gradually reduced and becomes random at the center of the tube (d). The cylinder axis of PI microdomains is found parallel to the perimeter of the tube.

near wall regions (Fig. 3(a)) indicates that global orientation of the cylindrical PI microdomains is obtained. No light was transmitted through crossed polarizers at the center regions (Fig. 3(d)), implying no microdomain orientation. The OM results confirmed that a global orientation was obtained during solvent evaporation in the cylindrical tube, and the best orientation occurred near the tube wall.

We investigated the effect of solvent evaporation rate on the orientation of PS/PI (45/12). Fig. 4 shows the two-dimensional SAXS patterns of PS/PI (45/12) samples cast

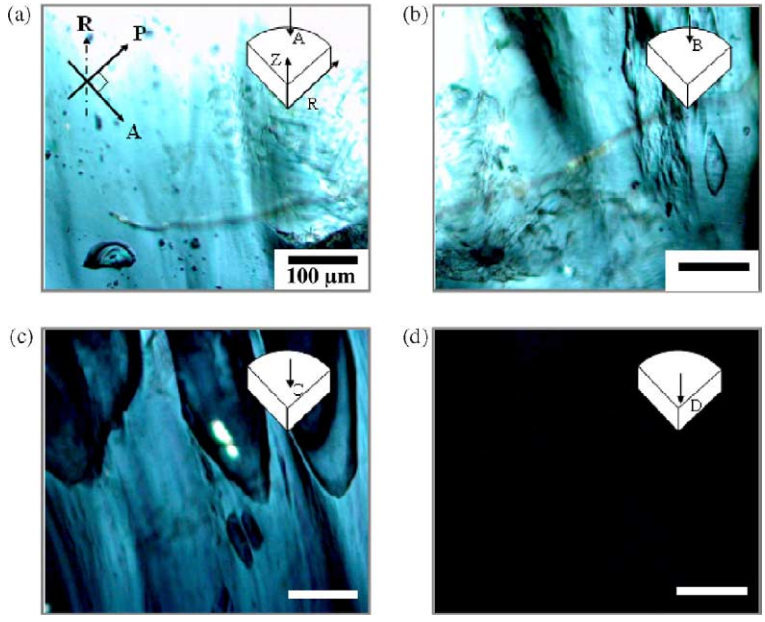

Fig. 3. Polarized optical microscope images of PS/PI (45/12) sample. Bright field images resulting from the form birefringence of the ordered cylindrical PI microdomains are obtained at 4 regions corresponding to Fig. 1(b). The tube wall regions show the brightest image, implying the maximum orientation of the cylindrical PI microdomains. No transmitted light image (d) confirms the random orientation at the center regions. A color filter was used that collects light with the wavelength of approximately 400–500 nm.

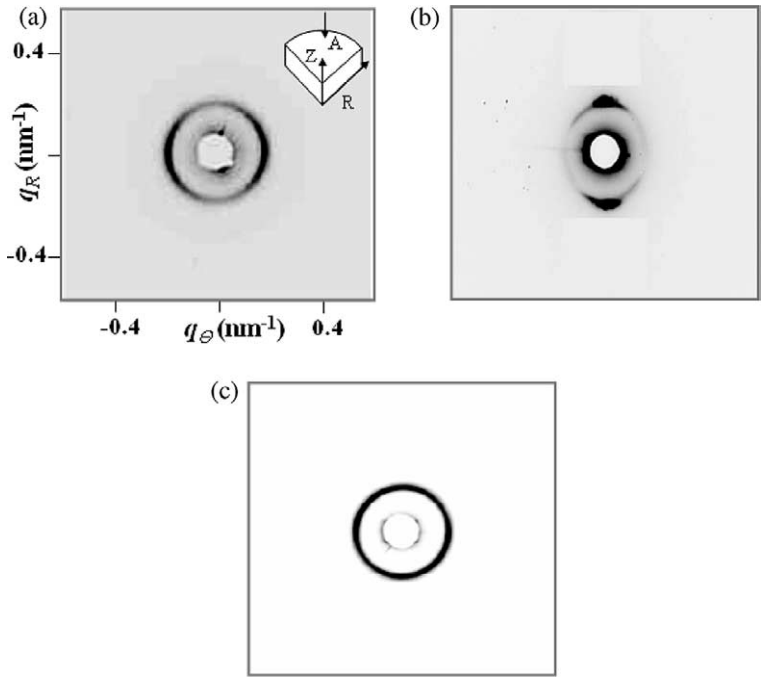

Fig. 4. 2D SAXS patterns of the solution cast PS/PI (45/12) with different solvent evaporation rates: (a) slow (~0.1 nL/s) (b) intermediate (~2.3 nL/s) (c) fast (~200 nL/s) with the incident beam parallel to the *Z* direction. Very weak and no orientation are observed with the fast and slow evaporation, respectively ((a) and (c)). The intermediate evaporation gives rise to a highly ordered microstructure of the cylindrical PI microdomains.

with the three different solvent evaporation rates: ~200 nL/s (a), ~2.3 nL/s (b) and ~0.1 nL/s (c). The incident beam was parallel to *Z*-axis and the scattering in the area near the wall was detected for all samples. Both fast and the slow evaporation did not produce the orientation of cylindrical PI microdomains. The solvent evaporation rate is one of the critical factors influencing orientation of block copolymer microdomains [10–14,21–23]. In thin poly(styrene-*b*-butadiene-*b*-styrene) block copolymer films (~100 nm in thickness), an intermediate evaporation (~5 nL/s) generated cylindrical PS microdomains vertically oriented to the film surface. In addition slow evaporation (~1.5 nL/s) produced in-plane cylinder [10]. In our case, PI cylinders vertically oriented with respect to the tube surface were hardly obtained due to large film thickness (~500 μm). Instead, PI cylinders tend to be oriented parallel to the tube surface. The in-plane cylindrical PI microdomains are oriented parallel to the perimeter of the tube wall.

In order to characterize the microstructure of the oriented PI microdomains more in detail, we performed SAXS with the incident beam perpendicular to the *RZ* plane. Fig. 5(a) shows the SAXS pattern of Fig. 4(b) with higher order reflections. The intensity scan across the meridian as a function of the scattering vector is shown in Fig. 5(c). The set of Bragg peaks have q_n/q_1 approximate values of 1, $\sqrt{3}$, $\sqrt{4}$, $\sqrt{7}$, $\sqrt{9}$, $\sqrt{12}$, etc. (the 1st peak is 0.18 nm^{-1} and the domain spacing is about 35 nm), which indicates a hexagonal lattice of the cylindrical PI microdomains. In our scattering pattern, $\sqrt{4}$ and $\sqrt{9}$ peaks are almost invisible. This is attributed from destructive interference of the form factor for cylindrical particle (due to intra-particle interference) and the angular positions at which such destructive interferences occur depend strongly on the volume fraction of cylinders (v). For instance, it has been shown from the scattering analysis for hexagonally arrayed cylindrical particles by Hashimoto et al. that the $\sqrt{3}$ peak being ascribed to (11) plane disappears when $v \cong 0.33$ even for perfectly arrayed hexagon and also that the $\sqrt{3}$ peak becomes dominant over other high order peaks as v decrease to smaller values [26]. In particular, their simulated scattering profile for $v \cong 0.27$, which is very close to the value in our case ($v \cong 0.25$), have revealed that the $\sqrt{4}$ and the $\sqrt{9}$ reflections are very weak whereas the $\sqrt{3}$ and the $\sqrt{7}$ peaks are relatively dominant over other high order peaks. Therefore, we infer that nearly extinct reflections at the $\sqrt{4}$ and the $\sqrt{9}$ are due mainly to the volume fraction of cylinder-forming PI block used in the study. In addition, paracrystal distortion of hexagon may also affect the relative intensities of high order peaks. Hashimoto et al. also have demonstrated through an isotropic distortion model for paracrystal distortion that the higher order peaks damped away to the asymptotic value of unity, more rapidly with increasing paracrystalline distortion [26]. In particular, the route $\sqrt{9}$ peak is significantly reduced in intensity. Since the ordered structure observed is kinetically driven in our current process, it is reasonable to expect that the hexagonal lattice is more or less distorted. This possibility is supported by the fact that the six-fold scattering pattern Fig. 5(b) is slightly distorted.

One can notice that the $\sqrt{3}$ peak ascribed to (11) plane is

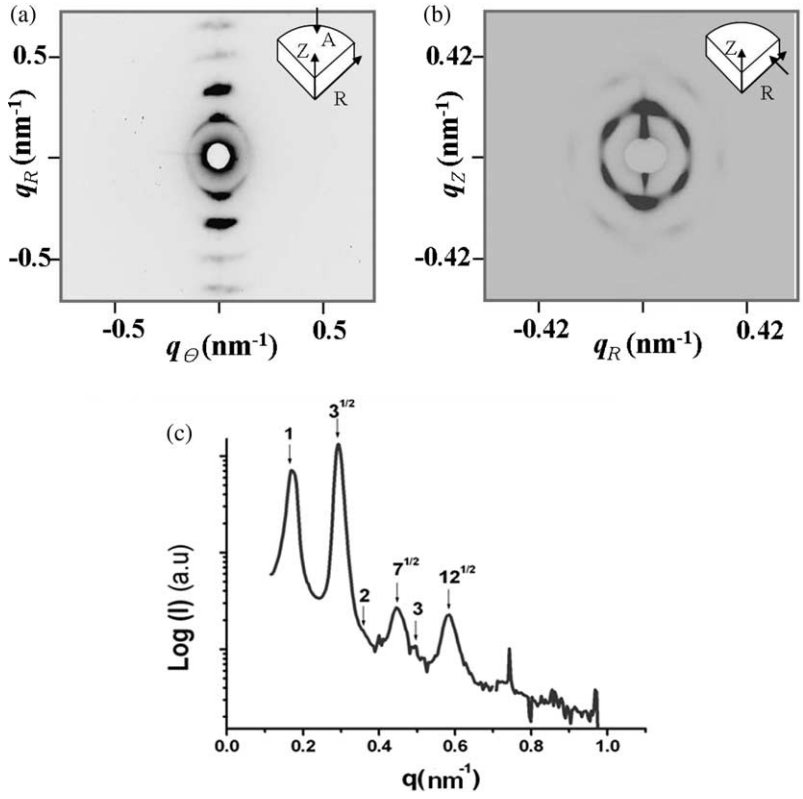

Fig. 5. 2D SAXS patterns of PS/PI (45/12) film cast with the intermediate evaporation rate. The tube wall regions are examined. (a) The SAXS image with the incident beam along the *Z* direction shows spot-like multiple reflections (b) The SAXS image with the incident beam along the perimeter of the tube (the scattering plane: *RZ* plane). The first and second reflections are shown with six-fold symmetry. (c) SAXS profile along the vertical (meridian) direction of (a) shows peaks in the ratio of 1, $\sqrt{3}$, $\sqrt{4}$, $\sqrt{7}$, $\sqrt{9}$, $\sqrt{12}$, indicating that the structure is characterized by a hexagonal packing of cylinders.

more intense than the first order peak to (10) one. This implies that (11) plane is dominantly aligned parallel to the incident beam. The SAXS pattern with the incident beam perpendicular to *RZ* plane (Fig. 5(b)) also exhibits that (10) plane is dominantly parallel to the bottom surface of the tube. The appearance of strong $\sqrt{12}$ peak that corresponds to (22) reflection, the second order (11) reflection supports our claim. Long range ordering of (11) plane parallel to the incident beam gives rise to the strong (22) scattering. One should note that (10) plane is also parallel to the tube wall at the regions very close to the tube wall. In fact, the best orientation shown in Fig. 5 took place in the regions slightly apart from the tube wall (approximately 100 μm). The order and the orientation of the cylindrical PI microdomains are not significantly altered over large area (a few hundred microns).

The ordered cylindrical PI microdomains in the regimes near the wall are visualized by TEM (Fig. 6). The PI microdomains, selectively stained with OsO_4, appear dark. A transverse view of the PI cylinder perpendicular to *R* direction is shown in Fig. 6(a). The in-plane cylindrical PI microdomains globally oriented parallel to the perimeter of the tube are clearly visible. The inset shows magnified image of the PI cylinder with a diameter of 20 nm and the average distance between the cylinders is 30–40 nm in agreement with the SAXS data. FFT image shown in the inset displays spot-like reflections located on the meridian, implying nearly single crystal like microstructure. The axial view of the structure parallel to the perimeter of the tube, perpendicular to *RZ* plane, shows that the PI microdomains clearly self-assembled onto a hexagonal lattice during the microphase separation under controlled solvent evaporation (Fig. 6(b)). The FFT power spectrum in the inset of Fig. 6(b) shows spot-like reflections with six-fold symmetry, indicating hexagonal packing of the PI microdomains.

We employed another block copolymer, PS/PI (44/19) that has a bicontinuous double gyroid structure. The block copolymer thick films were prepared with the intermediate evaporation rate in the cylindrical tube. The global orientation of the bicontinuous microdomains was also obtained in the regions near the tube wall. The 2D SAXS pattern with the incident beam parallel to the *Z* direction shows highly ordered spot-like multiple reflections (Fig. 7(a)). The azimuthal averaged intensity scan (Fig. 7(b)) presents the set of Bragg reflections with approximately relative *q* value of $\sqrt{6}$, $\sqrt{8}$, $\sqrt{20}$, $\sqrt{26}$, $\sqrt{30}$, $\sqrt{38}$ which corresponds to a gyroid ($Ia\bar{3}d$) structure. The inset of Fig. 7(a) shows SAXS pattern with different threshold cut-off to emphasize the first and second order reflections. The SAXS pattern obtained is similar to ones observed with the incident beam perpendicular to shear direction in the shear oriented gyroid samples where [111]

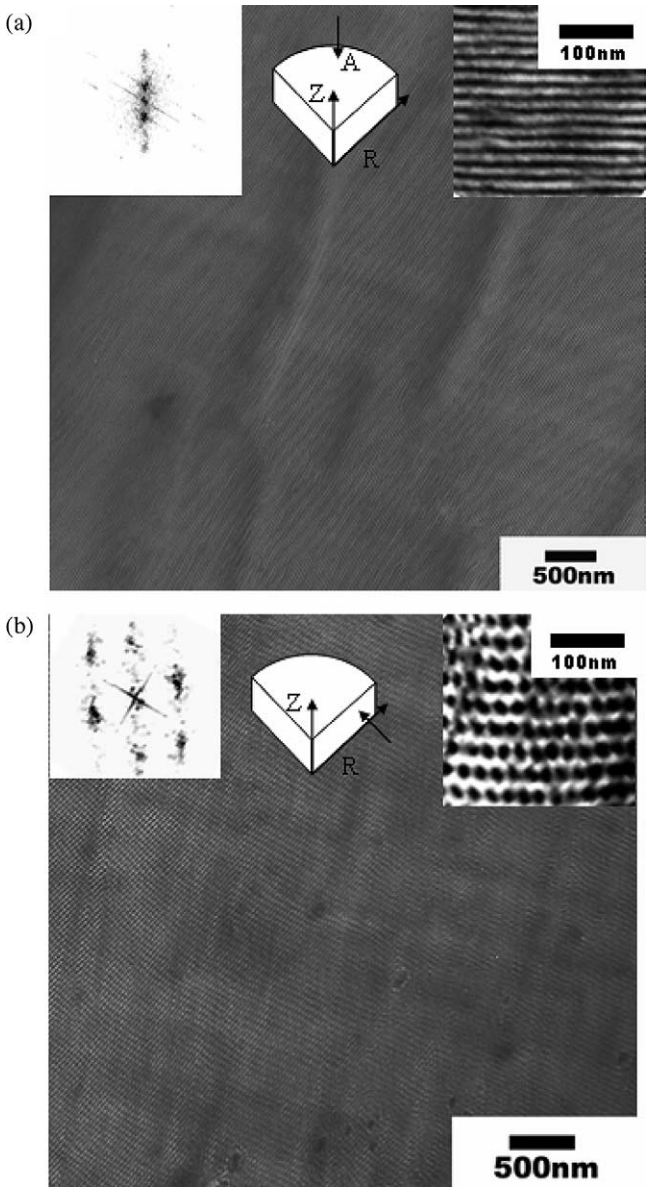

Fig. 6. Bright field TEM images of the microtomed sections of the solution cast PS/PI (45/12) films stained with OsO_4. (a) Transverse view showing PI cylinders aligned parallel to the perimeter of the tube. The inset image in the upper right side shows magnified cylindrical PI microdomains with approximately 20 nm in diameter. The fast Fourier transformation (FFT) pattern in the inset displays spot-like multiple reflections. (b) Axial view showing the hexagonal arrays of the cylindrical PI microdomains with their cylinder axis aligned parallel to the perimeter of the tube. The inset on the upper right side of (b) shows a magnified image of hexagonally packed cylindrical PI microdomains. FFT spectrum (inset on the upper left side) displays reflections with six-fold symmetry.

direction of the gyroid structures is parallel to the shear direction [27–30]. The SAXS pattern from individual single domains rotated randomly around the [111] directions provides typical 10 spot reflections [30–32]. In our sample, the [111] direction is parallel to the perimeter of the tube as evidenced by the presence of 10 spot reflections (inset of Fig. 7(a)). In fact $(2\bar{1}1)$ and $(\bar{2}1\bar{1})$ reflections are very weak.

The pattern indicates that scattering from single crystal domains with {211} and {220} crystal planes is dominant. Two strong second order {220} reflections on the meridian shown in the inset of Fig. 7(a) meet Bragg conditions. The rest shown in the inset are {211} reflections. It is noteworthy that the second order reflections corresponding to {220} ones are much stronger in intensity than the first order ones to {211} reflections (Fig. 7(b)). This implies that the single crystals with {220} plane parallel to the incident beam direction are dominant in our sample. Thomas et al. have demonstrated that {220} reflections are more intense than {211} reflections in the gyroid structure of a poly(styrene-*b*-isoprene-*b*-styrene) block copolymer oriented via roll casting [27]. Similar to our sample, the structure was highly ordered by the flow field induced by roll casting.

The ordered reflections appearing at low q regions ($\sim$0.09 nm^{-1}) correspond to {110} reflections of a cubic crystal which are supposed to be forbidden in gyroid symmetry (inset of Fig. 7(a)). During the solvent evaporation, the ordered structure was kinetically driven by the strong directional flow field, giving rise to the unique scattering. The reflections at lower q regions disappeared when the sample was annealed at 160 °C for 1 day. We currently make an effort to understand the structure. Higher order reflections from the gyroid phase are observed at $\sqrt{20}$, $\sqrt{26}$, $\sqrt{30}$, $\sqrt{38}$ which correspond to the allowed reflections for the $Ia\bar{3}d$ phase, {420}, {431}, {521} and the {611}, respectively. We used an automatic sample stage with which we scanned the sample with every 100 μm step. We found no significant orientation change in the scanned area of approximately 1 mm^2. The degree of orientation measured by full width half maximum (fwhm) of the strong {220} reflections gradually changed toward the center of the tube. The highly ordered region with fwhm of approximately 10° was preserved with the area of 500×500 μm^2. A photograph in Fig. 7(c) shows the highly ordered regions of the thick transparent PS/PI (44/19) film with approximately 1 mm^2 in area.

TEM of OsO_4 stained sections permits direct visualization of the PI microdomains in the ordered double gyroid sample. The TEM projection along the Z direction, which corresponds to the scattering plane of Fig. 7(a), is shown in Fig. 8(a). Nearly single crystal gyroid structure was seen. The ordered domains are extended to several hundred micrometers. Because it was difficult to microtome the samples with the section plane exactly perpendicular to the Z direction, the preferential {220} reflections observed in the SAXS pattern was hardly obtained. Instead, TEM micrograph contains the microstructures of the planes perpendicular to both {220} and {211} crystal planes. The microstructure shown in Fig. 8(a) is very similar to a simulated TEM image of gyroid structure projected along [011] direction (inset of Fig. 8(a)). Both $(21\bar{1})$ and $(0\bar{2}2)$ planes are parallel to [011] direction, which is consistent with the scattering data shown in Fig. 7(a). The TEM projection along the perimeter of the tube on the RZ plane (Fig. 8(b)) clearly exhibits globally ordered three-fold

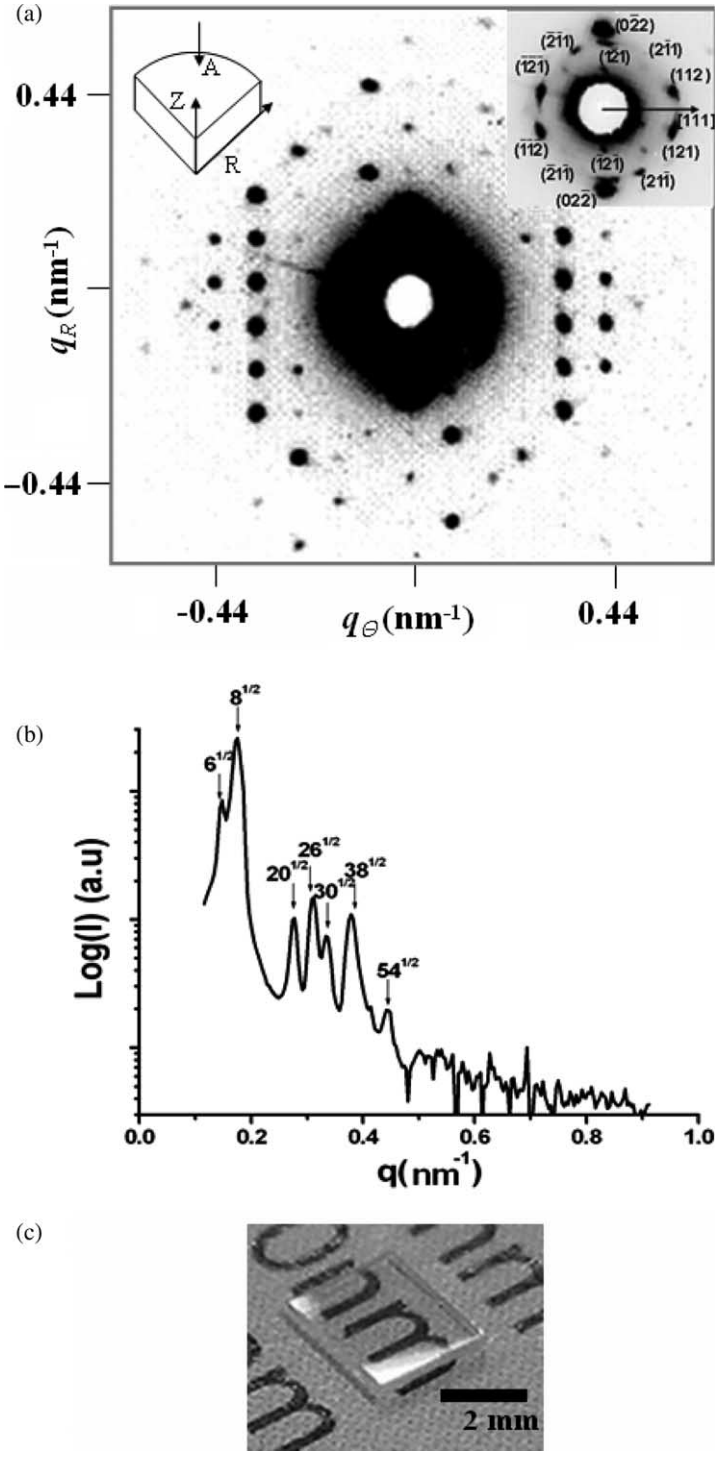

Fig. 7. (a) 2D SAXS pattern of PS/PI (44/19) film cast with the intermediate evaporation rate. The incident beam is parallel to the *Z* direction and the film near the tube wall regions is examined. The pattern exhibits spot-like multiple reflections of a bicontinuous double gyroid cubic structure ($Ia\bar{3}d$). The inset with different threshold cut-off emphasizes the first and second order reflections. The scattering reflections from single crystal domains with {211} and {220} planes of a double gyroid structure are apparent. (b) Azimuthal averaged SAXS profile confirms the bicontinuous double gyroid structure with the peaks in the ratio of $\sqrt{6}$, $\sqrt{8}$, $\sqrt{20}$, $\sqrt{26}$, $\sqrt{30}$, $\sqrt{38}$. (c) A photograph of transparent PS/PI (44/19) film with highly ordered microstructure. The areas near tube wall regions are chosen.

wagon wheel structure typically observed in the projection along the [111] direction of a gyroid phase [33]. A simulated TEM image along [111] direction also exhibits three-fold symmetry (inset of Fig. 8(b)).

In the case of PS/PI (45/12), cylindrical PI microdomains are in-plane on the surface of the tube, and globally oriented with their cylinder axis parallel to the perimeter of the tube. The highest orientation occurred near the tube wall at the

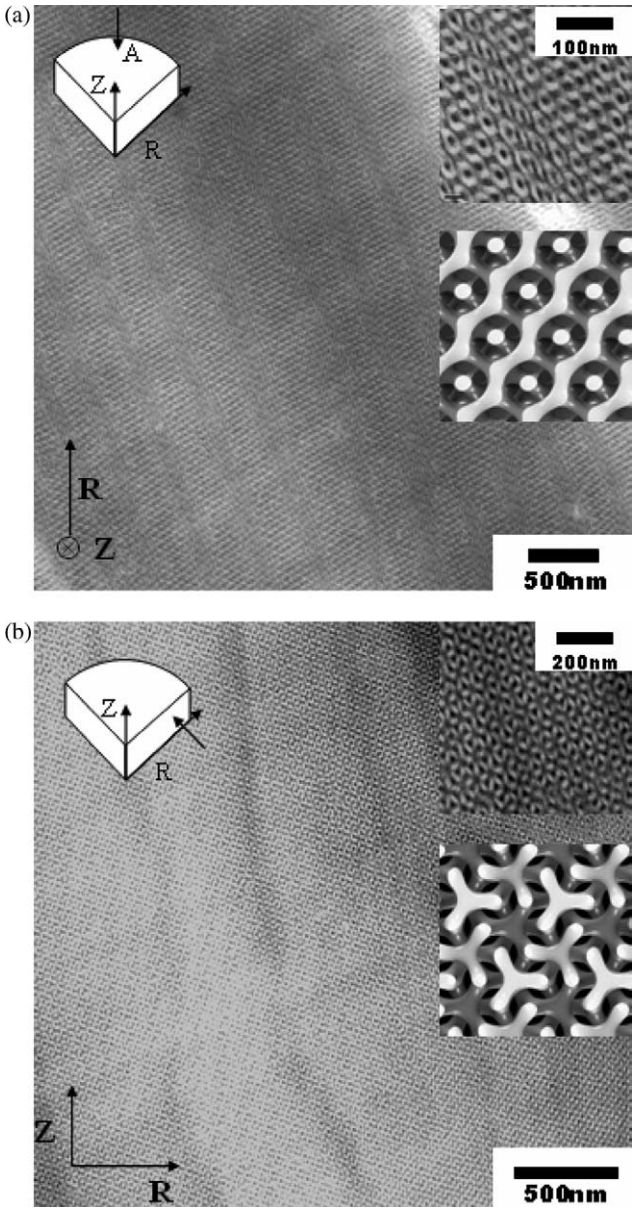

Fig. 8. Bright field TEM images of the microtomed sections of the solution cast PS/PI (44/19) films stained with OsO_4. (a) The sectioned film surface is perpendicular to the *Z* direction. Highly ordered microstructure of a gyroid structure projected along both ⟨211⟩ and ⟨220⟩ directions is observed. The ordering is produced over several hundred micrometers. The inset shows a magnified ordered cubic phase (the upper image) and a simulated TEM image of gyroid structure projected along [011] direction (the lower one). (b) The sectioned film surface is normal to the perimeter of the tube. TEM image projected on *RZ* plane exhibits a globally ordered three-fold wagon wheel structure. The inset shows a magnified three-fold cubic structure (the upper image) and a simulated TEM image of gyroid structure projected along [111] direction (the lower one).

intermediate evaporation rate. There exist two orthogonal external forces: (1) The flow of the solution within a meniscus directed toward the tube wall and (2) the solvent evaporation that forces the ordering front to initiate at the surface of the solution and propagate into the solution.

Our method is very similar to one using strong capillary forces at a meniscus between a substrate and a colloidal sol to induce crystallization of sphere into a 3D array of controllable thickness [34–36]. Evaporation of the solvent out of the meniscus leads to a constant solution influx, which draws colloids into the area of film formation. The same principle has been successfully applied to the formation of surfactant-templated inorganic materials [37]. In our current systems, we used block copolymer solutions, which undergo microphase separation at a certain solution concentration during solvent evaporation. The higher evaporation rate at the edge of a meniscus gives rise to the gradient of evaporation rate, which subsequently induces the flow of a solution toward the tube wall. At a certain critical order-disorder solution concentration (C_{ODT}) during solvent evaporation, the microphase separation of the block copolymer begins at the air-block copolymer solution interface, in particular at the edge of the meniscus and propagate toward the center regions. Continuous evaporation of the solvent induces the microstructure orientation along the *Z*-direction as well. Hexagonal arrays of in-plane PI cylinders parallel to the bottom surface of the tube are aligned with their cylindrical axis parallel to the perimeter of the tube at the intermediate evaporation rate. The slow evaporation rate does not generate a sufficient gradient of evaporation rate at the edge of a meniscus, resulting in randomly ordered in plane PI cylinders. With the fast evaporation rate, almost zero gradient of the evaporation rate is formed and the microstructure consists of polygrains. It should be noted that even with the intermediate rate there is no lateral orientation at the center of the film and instead randomly oriented in-plane PI cylinders were observed.

Another strong driving force for orienting block copolymer microdomains is shear strain induced by the directional solvent evaporation [38,39]. Hu and Larson have recently studied the effect of stresses on the microflow in an evaporating droplet and analytically solved the evaporation flux and temperature profiles along the droplet surface. In our system, the shear stress induced during evaporation near tube wall significantly affected the morphology of the block copolymers. In fact strong molecular chain stretching was observed in the regions very near the tube wall. It was confirmed by X-ray scattering experiment with the incident beam parallel to Z-axis where the scattering vector, q of the first order (10) reflection gradually decreases toward the wall. The lattice deformation of approximately 25%, caused by the strong shear field, was obtained very near the wall (data not shown).

In the case of PS/PI (44/19), we obtained the microstructure orientation where [111] direction of a gyroid phase is parallel to the perimeter of the tube. The {211} planes of the gyroid structure were epitaxially related to the {10} plane of hexagonally packed cylinders observed in lyotropic systems and several block copolymer systems [28–30]. Lodge et al. have extensively studied the phase transition of block copolymer solution recently [28,29]. A symmetric diblock copolymer undergoes direct disorder to

ordered lamellae structure during solvent evaporation only when the solvent is perfectly neutral for both blocks. In general this condition rarely meets in most of block copolymer solutions including ours. Thus homogeneous block copolymer solutions are first transformed into disordered micelle phase followed by ordered sphere, cylinder, bicontinuous gyroid and finally lamellae one. The cylindrical axis in hexagonal phase is transformed into [111] in a gyroid during order–order transition. The microstructures obtained in both PS/PI (45/12) and PS/PI (44/19) have the main axes: The PI cylinder axis for PS/PI (45/12) and the [111] direction of the gyroid structure for PS/PI (44/19) parallel to the tube perimeter. With the consideration of the epitaxial relationship between the two phases, the biaxial driving forces in our method were exerted on the orientation of both block copolymers with the same manner.

The solvent significantly affected the orientation of microdomains. We prepared the PS/PI (45/12) block copolymer films cast from either xylene or THF. We chose xylene because its boiling temperature is close to toluene (130 °C). Whereas THF has a low boiling temperature that causes fast evaporation. We found that the samples prepared from xylene exhibited the similar orientation to one observed in the samples from toluene. However, long range ordering was significantly reduced. In contrast, THF as a selective solvent for PS with higher vapor pressure led to a more rapid migration of an ordering from the free surface that resulted in no efficient flow of the solution toward the tube wall. Random orientation of the cylindrical PI microdomains was observed similar to one obtained from toluene with the fast evaporation rate.

We also examined different cylinder forming block copolymer films such as poly(styrene-*b*-ethylenepropylene) (PS-*b*-PEP), poly(styrene-*b*-methylmethacrylate) (PS-*b*-PMMA) and poly(styrene-*b*-vinylpyridine) (PS-*b*-PVP) prepared from toluene. For all three block copolymers, cylindrical microdomains in PS matrix are formed. PS-*b*-PEP showed the long range orientation similar to one previously observed in PS/PI (45/12) while the other two block copolymers exhibited very weak orientation. In the current system, we should consider three interaction parameters such as ones between block A and solvent, between block B and solvent, and between block A and B. In addition, the orientation of microdomains is significantly influenced by interfacial interaction: Air–polymer and substrate–polymer. Kimura et al. demonstrated that MEK which is a selective solvent for PS block made both PBD and PS components present at the PBD preferential substrate surface due to the higher solubility of PS and the reduced difference in the surface energies of components [14]. They obtained a highly ordered microstructure during evaporation in combination with solvent pinning. In our system, since the microphase separation initiates at the air/block copolymer solution interface and the final film thickness is large ($\sim$500 μm), the contribution of the block copolymer/tube surface interfacial energies to the orientation is relatively small. Interplay of the interactions among blocks and solvent and the interfacial energies needs to investigate in the future.

4. Conclusions

The solution flow induced by the strong capillary force at a meniscus between the cylindrical tube wall and the block copolymer solution coupled with solvent evaporation provides a simple way to generate well-ordered cylindrical or bicontinuous microdomains in thick block copolymer films. The hexagonal arrays of in-plane cylindrical microdomains with respect to the bottom surface are aligned with their cylinder axis parallel to the perimeter of the tube. In the case of PS/PI (44/19) with a bicontinuous gyroid microstructure, crystallographic [111] direction of the gyroid structure is parallel to the perimeter of the tube. {220} Planes of the gyroid structure are found to be dominantly perpendicular to the bottom surface of the tube. The capillary forces at the meniscus cause a directional flow of the block copolymer solution toward the tube wall. The solvent evaporation initiates the microphase separation of the block copolymer at the air–solution interface and propagates into the interior of the solution. Our simple route can allow to fabricate nanopatterned porous membranes or replica stamps when one of the block is removed by ozone or/and ultraviolet selectively.

Acknowledgements

We thank Prof M. S. Lee, Mrs J. H. Song, Mr J. H. Kim and Dr K. W. Kim for their assistances of TEM and SAXS experiments. We are grateful for helpful conversations with Mr B. Kim at KIST. We also thank Dr L.J. Fetters for synthesizing the block copolymers. This research was supported by Ministry of Science and Technology, the Republic of Korea, for financial support through Fusion Technology Program.

References

[1] Bates FS, Frederickson GH. Annu Rev Phys Chem 1990;41:525.
[2] Park C, Yoon J, Thomas EL. Polymer 2003;44:6725.
[3] Hamley IW. Angew Chem Int Ed 2003;42:1692.
[4] Thurn-Albrecht T, Schotter J, Kastle GA, Emley N, Shibauchi T, Krusin-Elbaum L, et al. Science 2000;290:2126.
[5] Elhadj S, Woody JW, Niu VS, Saraf RF. Appl Phys Lett 2003;82:871.
[6] Xiang H, Lin Y, Russell TP. Macromolecules 2004;37:5358.
[7] Albalak RJ, Thomas EL, Capel MS. Polymer 1998;38:3819.
[8] Park C, De Rosa C, Fertters LJ, Thomas EL. Macromolecules 2000; 33:7931.
[9] Villar MA, Rueda DR, Ania F, Thomas EL. Polymer 2002;43:5139.
[10] Kim G, Libera M. Macromolecules 1998;31:2569.

[11] Fukunaga K, Elbs H, Maerle R, Krausch G. Macromolecules 2000;33:947.
[12] Lin Z, Kim DH, Wu X, Boosahda L, Stone D, LaRose L, et al. Adv Mater 2002;14:1373.
[13] Kim SH, Misner M, Xu T, Kimura M, Russell TP. Adv Mater 2004;16:226.
[14] Kimura M, Misner MJ, Xu T, Kim SH, Russell TP. Langmuir 2003;19:9910.
[15] Segalman RA, Yokoyama H, Kramer EJ. Adv Mater 2001;13:1152.
[16] Cheng JY, Ross CA, Thomas EL, Smith HI, Vancso GL. Appl Phys Lett 2002;81:3657.
[17] Kim SO, Solak HH, Stoykovich MK, Ferrier NJ, De Pablo JJ, Nealey PF. Nature 2003;424:411.
[18] Sundrani D, Darling SB, Sibener SJ. Nano Lett 2004;4:27.
[19] Hashimoto T, Bodycomb J, Funaki Y, Kimishima K. Macromolecules 1999;32:952.
[20] Bodycomb J, Funaki Y, Kimishima K, Hashimoto T. Macromolecules 1999;32:2075.
[21] De Rosa C, Park C, Thomas EL, Lotz B. Nature 2000;405:433.
[22] Park C, De Rosa C, Thomas EL. Macromolecules 2001;34:2602.
[23] Park C, Cheng JY, De Rosa C, Fasolka MJ, Mayes AM, Ross CA. Appl Phys Lett 2001;79:848.
[24] Deegan RD, Bakajin O, Dupont TF, Huber G, Nagel SR, Witten TA. Nature 1997;389:827.
[25] Cavicchi KA, Lodge TP. Macromolecules 2004;37:6004.
[26] Hashimoto T, Kawamura T, Harade M, Tanaka H. Macromolecules 1994;27:3063.
[27] Dair BJ, Avgeropoulos A, Hadjichristidis N, Capel M, Thomas EL. Polymer 2000;41:6231.
[28] Wang C, Lodge TP. Macromol Rapid Commun 2002;23:49.
[29] Wang C, Lodge TP. Macromolecules 2002;35:6997.
[30] Hamley IW. J Phys: Condens Matter 2001;13:643.
[31] Forster S, Khandpur AK, Zhao Z, Bates FS, Hamley IW, Ryan AJ, et al. Macromolecules 1994;27:6922.
[32] Vigild ME, Almdal K, Mortensen K, Hamley IW, Faircloughb JPA, Ryan AJ. Macromolecules 1998;31:5702.
[33] Hasegawa H, Tanaka H, Yamasaki K, Hashimoto T. Macromolecules 1987;20:1651.
[34] Vlasov YA, Bo XZ, Sturm JC, Norris DJ. Nature 2001;414:289.
[35] Jiang P, Bertone JF, Hwang KS, Colvin VL. Chem Mater 1999;11:2123.
[36] Dimitrov AS, Nagayama K. Langmuir 1996;12:1303.
[37] Grosso D, Cagnol F, Soler-Illia GJDAA, Crepaldi EL, Amenitsch H, Brunet-Bruneau A, et al. Adv Funct Mater 2004;14:309.
[38] Hu H, Larson RG. Langmuir 2005;21:3972.
[39] Hu H, Larson RG. Langmuir 2005;21:3963.